

A Generalized Equivalence Method for the Calculation of Low-Frequency EMI on Pipeline Networks
Considering Polarization Effect

Original

A Generalized Equivalence Method for the Calculation of Low-Frequency EMI on Pipeline Networks Considering Polarization Effect / Liu, Minzhou; Xie, Yan-zhao; Wu, Yu-ying; Trincherò, Riccardo; Stievano, Igor Simone. - In: IEEE TRANSACTIONS ON POWER DELIVERY. - ISSN 0885-8977. - STAMPA. - (2024), pp. 1-13.
[10.1109/tpwrd.2024.3378924]

Availability:

This version is available at: 11583/2987145 since: 2024-03-20T08:45:42Z

Publisher:

IEEE

Published

DOI:10.1109/tpwrd.2024.3378924

Terms of use:

This article is made available under terms and conditions as specified in the corresponding bibliographic description in the repository

Publisher copyright

IEEE postprint/Author's Accepted Manuscript

©2024 IEEE. Personal use of this material is permitted. Permission from IEEE must be obtained for all other uses, in any current or future media, including reprinting/republishing this material for advertising or promotional purposes, creating new collecting works, for resale or lists, or reuse of any copyrighted component of this work in other works.

(Article begins on next page)

A Generalized Equivalence Method for the Calculation of Low-Frequency EMI on Pipeline Networks Considering Polarization Effect

Min-zhou Liu, *Member, IEEE*, Yan-zhao Xie, *Senior Member, IEEE*, Yu-ying Wu, Riccardo Trincherò, *Member, IEEE*, and Igor Simone Stievano, *Senior Member, IEEE*

Abstract—Large-scale pipeline networks may be subject to wide-area and spatially nonuniform external electromagnetic interference. This paper presents a generalized and efficient algorithm for the calculation of inductive and conductive coupling to pipeline networks based on the two-port equivalent circuit. In the modified transmission line model of the pipeline, the external interference are characterized by using only longitudinal voltage sources. In addition, the nonlinear polarization of coating breakdown is incorporated into the circuit model of the network. The linear pipe segments can be independently reduced to the equivalent- π circuit with analytical parameters, which enables model order reduction of the network. Such techniques can be applied to arbitrary nonuniform excitation fields. Several test cases are used to illustrate the response characteristics of pipelines excited by interference with different spatial patterns, including geomagnetic disturbances and HVDC earth return currents.

Index Terms—Conductive coupling, equivalent- π circuit, geomagnetic disturbances, HVDC earth return currents, inductive coupling, polarization effect, transmission line model.

I. INTRODUCTION

Oil and gas pipeline networks are subject to various low-frequency external electromagnetic interference (EMI). Especially nowadays, pipelines and other energy infrastructures are built in increasingly confined spaces, such as common corridors with power lines; thus the pipelines may be continuously exposed to strong EMI stresses. The resulting voltage and current responses may accelerate the corrosion of pipelines and interfere with cathodic protection devices, etc. Assessing their electromagnetic effects and deploying cost-effective mitigation measures have long been topics of interest in engineering practice. Rigorous evaluation of the

This work was supported in part by the National Key R&D Program of China under Grant 2023YFE0115700, in part by the China Scholarship Council under Grant 202006280077, and in part by the Outstanding Chinese and Foreign Youth Exchange Program of China Association for Science and Technology (CAST). (*Corresponding author: Yan-zhao Xie.*)

Min-zhou Liu is with the State Key Laboratory of Electrical Insulation and Power Equipment, School of Electrical Engineering, Xi'an Jiaotong University, Xi'an 710049, China, and also with the Department of Electronics and Telecommunications, Politecnico di Torino, 10129 Turin, Italy (e-mail: liuminzhou@outlook.com).

Yan-zhao Xie and Yu-ying Wu are with the State Key Laboratory of Electrical Insulation and Power Equipment, School of Electrical Engineering, Xi'an Jiaotong University, Xi'an 710049, China (e-mail: yzxie@mail.xjtu.edu.cn; yywu626@stu.xjtu.edu.cn).

Riccardo Trincherò and Igor Simone Stievano are with the Department of Electronics and Telecommunications, Politecnico di Torino, 10129 Turin, Italy (e-mail: riccardo.trincherò@polito.it; igor.stievano@polito.it).

electromagnetic response in the pipeline network is the first step to support this work.

Low-frequency EMI to pipelines can be electrically classified into three categories: *capacitive*, *inductive* and *conductive* [1], [2]. For buried pipelines, the capacitive coupling occurs only for pipelines exposed during installation or maintenance, and can generally be ignored during normal operation due to the shielding effect of the ground. Thus, this paper mainly focuses on the latter two coupling mechanisms. The inductive coupling is caused by time-varying magnetic flux generated by external current sources, e.g., fundamental frequency AC and harmonic currents in nearby power lines [3]–[7], ionospheric source currents associated with geomagnetic activity [8]–[13], etc. The conductive coupling is triggered by the soil potential rise due to ground fault currents from the power grid [14], [15], HVDC earth return currents [16]–[21], metro stray currents [22], etc.

The external electromagnetic environment may have a wide footprint with spatially nonuniform distribution. For instance, the currents from the HVDC electrodes can affect pipelines several kilometers away, and geomagnetic disturbances initiated by space weather can produce interference on even continental levels. Moreover, the affected pipeline networks to be evaluated are usually large-scale and multi-branch.

A. Related Work and Motivation

EMI coupling to buried pipelines can usually be analyzed by using the transmission line (TL) model with distributed parameters. Noteworthy here is that the arrangement of the excitation source is different in the circuits used for inductive and conductive coupling: the former is in the longitudinal branch, whereas the latter is in the transverse branch. Taflove *et al.* [3] proposed the TL model for the inductive coupling of pipelines resulting from nearby power lines. The model was subsequently extended by Boteler and Cookson [8] for geomagnetic induction in pipelines. Lagace *et al.* [16] proposed the TL model for the conductive interference caused by HVDC earth return currents.

Analytical solutions for voltage and current responses can be acquired simply for a single pipeline, however, it is difficult for networks with complex topology. The nodal voltage analysis based on discretization of pipelines [1], [15], [19] usually yields large-scale computational models. In contrast, the equivalence-based algorithms [3], [9], [10], [12], [23] become a more efficient scheme.

Several equivalence methods have been developed specifically for inductive or conductive coupling to a pipeline. An equivalent Thévenin circuit is normally adopted for the single-port equivalence of a pipeline to analyze the inductive coupling due to AC power lines [3] and geomagnetic disturbances [9]. It usually starts from a pipe located at the edge of the network and is then performed sequentially according to the network topology. In addition, an equivalent- π circuit was proposed for the two-port equivalence of the pipeline excited by external electric fields, and the analytical solutions of its parameters were derived in the cases of uniform [10] and nonuniform [12] geoelectric field induced by geomagnetic disturbances. The two-port equivalence can be applied to each single-conductor pipeline individually, which is more suitable for large-scale networks.

Some efforts have been made for the unified modeling of inductive and conductive coupling. Haubrich *et al.* [23] presented a universal two-port equivalent model for inductive and conductive interference through voltage and current transformations. However, it assumes that the electric field along each pipeline is constant.

Furthermore, the literature on pipeline equivalents mentioned above assume the linearity of all elements in the network while ignoring the nonlinear polarization of coating breakdown [24]. The results given by Li *et al.* [20], [21] show that the neglect of nonlinear polarization can result in rather conservative estimates of the responses for the analysis of HVDC earth return currents, which implies uneconomic mitigation measures.

B. Our Contributions

To address the above issues, this paper proposes a more general modeling and equivalence technique for the EMI analysis of large-scale pipeline networks. The novel algorithm has the following advantages:

- 1) The modified TL model of the pipeline is capable of handling the inductive or conductive EMI as well as the co-existence of both, which are characterized as only single longitudinal voltage source in terms of electric fields.
- 2) The pipeline network is divided into linear pipe segments and nonlinear grounded branches due to locally damaged coatings. The linear pipe segment excited by electric fields can be reduced to an equivalent- π circuit. It is applicable to arbitrary nonuniform electric fields without necessarily being constant or in a specific function form.
- 3) The nodal voltage analysis can be performed more efficiently for large-scale pipeline networks with nonlinear polarization, given each linear pipeline segment has been simplified as a lumped circuit, thus considerably reducing the model order of the system of nonlinear equations to be solved.

The rest of this paper is organized as follows. Section II discusses the generalized TL model of a pipeline for inductive and conductive EMI analysis. Section III details the proposed algorithm to solve the voltage and current responses of a

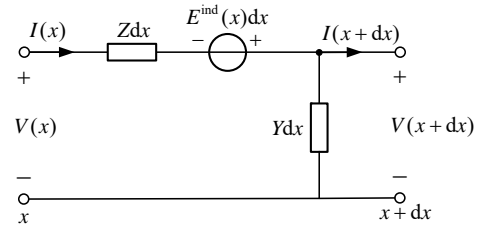


Fig. 1. Equivalent TL circuit of a pipeline affected by inductive interference.

pipeline network considering nonlinear polarization effect. In Section IV, the proposed algorithm is validated with field test results. Then, Section V presents several illustrative pipeline network cases subjected to the geomagnetic disturbances and HVDC earth return currents, as typical examples of inductive and conductive interference, respectively. Finally, Section VI concludes the paper.

II. GENERALIZED MODELING OF A PIPELINE FOR INDUCTIVE AND CONDUCTIVE COUPLING

A. Inductive Coupling Model of Pipeline

The cause of inductive coupling is the magnetic coupling of external source currents to the pipe. It thus induces electric fields according to Faraday's law of induction, which in turn drive stray currents in the pipe.

Let us assume that the pipe is along the x -axis, then a single cell equivalent structure of a pipe excited by electric fields is depicted in Fig. 1. The *remote earth* at infinite depth is taken as the potential reference point. The voltage of the metal tube to the remote earth is denoted as V and the longitudinal current along the pipeline is I . The tangential electric field at location x induced by the external source current along the pipeline is denoted as $E^{\text{ind}}(x)$, which can be modeled as distributed voltage sources in the longitudinal branch of the circuit. Accordingly, the TL equations for inductive coupling can be written as [3]

$$\frac{dV(x)}{dx} + ZI(x) = E^{\text{ind}}(x) \quad (1)$$

$$\frac{dI(x)}{dx} + YV(x) = 0 \quad (2)$$

where Z and Y are the per-unit-length longitudinal impedance and transverse admittance, respectively. The transverse admittance Y is contributed by both the coating and the soil [16], and the former is usually much lower than the latter for well-insulated pipes.

B. Conductive Coupling Model of Pipeline

The conductive EMI is generated by the soil potential difference along the pipeline due to external grounding currents. It can also be modeled based on TL theory, as shown in the top panel of Fig. 2.

In the original TL circuit model, the *remote earth* at infinity depth is taken as the potential reference point. The coating can be considered as a branch with a large resistance between the soil and the metal tube. The soil potential rise at location x

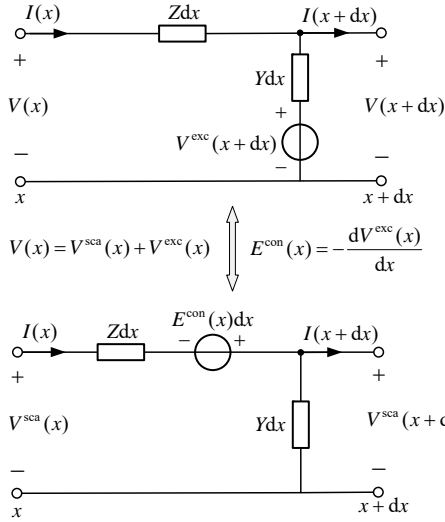


Fig. 2. Original (top) and modified (bottom) TL circuit models of a pipeline affected by conductive interference.

along the pipeline due to the external earthing current, namely the excitation voltage $V^{\text{exc}}(x)$, can be modeled as a transverse voltage source in the circuit. The voltage of the metal side of the coating to the remote earth is denoted as $V(x)$. Thus, the TL equations for the conductive coupling are given by [16]

$$\frac{dV(x)}{dx} + ZI(x) = 0 \quad (3)$$

$$\frac{dI(x)}{dx} + YV(x) = YV^{\text{exc}}(x) \quad (4)$$

We can find that for inductive and conductive coupling, the voltage source is placed on the longitudinal and transverse branches in the original TL circuit, respectively. Correspondingly, the source term is imposed in the first and second TL equation, respectively.

The original TL equations are about the voltage $V(x)$ of the metal side to the remote earth. We can treat the excitation voltage on the soil side of the coating as *local earth*. Then, the voltage $V(x)$ can be decomposed into two parts as in (5), namely, the scattered voltage $V^{\text{sca}}(x)$ on the metal side to local earth, and the excitation voltage $V^{\text{exc}}(x)$ to remote earth. In this case, the excitation voltages are created by the external source currents, whereas the scattered voltages [25] are created by other currents and charges in the pipeline and the ground.

$$V(x) = V^{\text{sca}}(x) + V^{\text{exc}}(x) \quad (5)$$

Moreover, the tangential electric field $E^{\text{con}}(x)$ along the pipe generated by the external earthing current can be expressed as a negative gradient of the excitation voltage:

$$E^{\text{con}}(x) = -\frac{dV^{\text{exc}}(x)}{dx} \quad (6)$$

Substituting (5) and (6) into the original TL equations (3)-(4), the modified TL equations about the scattered voltage

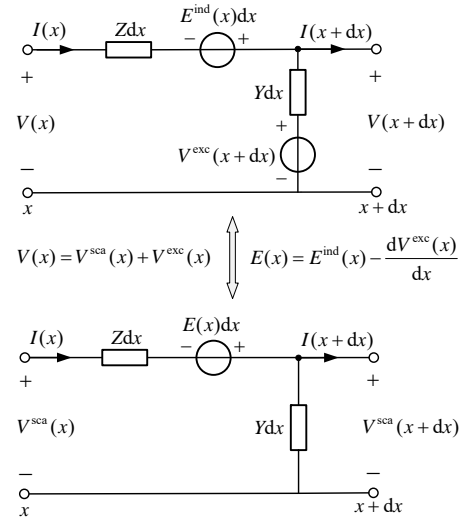


Fig. 3. Original (top) and modified (bottom) TL circuit models of a pipeline affected by both inductive and conductive interference.

$V^{\text{sca}}(x)$ can be derived as

$$\frac{dV^{\text{sca}}(x)}{dx} + ZI(x) = E^{\text{con}}(x) \quad (7)$$

$$\frac{dI(x)}{dx} + YV^{\text{sca}}(x) = 0 \quad (8)$$

We can find that the modified TL equations (7)-(8) for conductive coupling have the same form as those for inductive coupling in (1)-(2), which yields a modified circuit as depicted in the bottom panel of Fig. 2.

In addition, the original TL model of *capacitive coupling* [5], although not discussed in detail in this paper, is similar to that of conductive coupling. Thus, the circuit transformation in this subsection is also applicable to the capacitive coupling.

C. Pipeline Affected by Both Inductive and Conductive EMI

Pipelines may be subject to both inductive and conductive EMI in some scenarios. For instance, an AC power line may have a ground fault near the pipe [14], [15], or geomagnetic disturbances and HVDC earth return currents may occur simultaneously [26]. Thus, the sources are present both longitudinally and transversely in the original circuit model, as shown in the top panel of Fig. 3. Correspondingly, both TL equations are imposed with the source term:

$$\frac{dV(x)}{dx} + ZI(x) = E^{\text{ind}}(x) \quad (9)$$

$$\frac{dI(x)}{dx} + YV(x) = YV^{\text{exc}}(x) \quad (10)$$

In this case, the voltage and current responses of the pipe are contributed by both the induced electric field E^{ind} in the pipe and the soil potential rise V^{exc} . We can use the total exciting electric field E tangential to the pipe, which is the sum of the inductive part E^{ind} and the conductive part E^{con} :

$$E(x) := E^{\text{ind}}(x) + E^{\text{con}}(x) = E^{\text{ind}}(x) - \frac{dV^{\text{exc}}(x)}{dx} \quad (11)$$

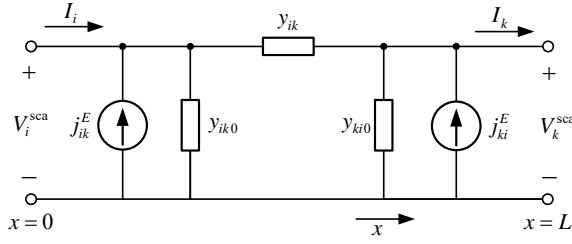


Fig. 4. Equivalent-pi circuit of a pipeline excited by external electric fields.

It allows us to obtain the modified TL equations about the scattered voltages, which are defined in (5), as follows:

$$\frac{dV^{\text{sca}}(x)}{dx} + ZI(x) = E(x) \quad (12)$$

$$\frac{dI(x)}{dx} + YV^{\text{sca}}(x) = 0 \quad (13)$$

The above equations can be regarded as a general form of (1)-(2) for the inductive coupling and (7)-(8) for the conductive coupling analysis. For purely inductive coupling, we have $V(x) = V^{\text{sca}}(x)$. In summary, by modifying the TL model, the excitation is unified as the only longitudinal voltage source in terms of the electric fields. This transformation is applied to arbitrary spatially nonuniform induced fields E^{ind} and soil excitation potential V^{exc} . Furthermore, the simplified equivalent method proposed in our earlier work [12] for inductive coupling of pipelines can be extended to the analysis of other types of EMI.

In addition, the modified TL equations (12)-(13) are about the scattered voltages $V^{\text{sca}}(x)$, which is proportional to the leakage current density $i^{\text{leak}}(x)$ and pipe-to-soil potential (PSP) $V^{\text{psp}}(x)$ as in (14)-(15). For well-insulated pipelines, i.e. when the resistivity of the coating is far larger than that of the soil, the approximation $V^{\text{psp}}(x) \approx V^{\text{sca}}(x)$ is generally considered valid. Thus, $V^{\text{sca}}(x)$ is more concerned in engineering practice compared to the total voltage $V(x)$ to the remote earth in the original TL equations (9)-(10).

$$i^{\text{leak}}(x) = \frac{YV^{\text{sca}}(x)}{2\pi r} \quad (14)$$

$$V^{\text{psp}}(x) = \frac{Y}{Y_{\text{coat}}} V^{\text{sca}}(x) \quad (15)$$

where r and Y_{coat} are the outer radius and transverse admittance of the insulation coating, respectively.

III. THEORETICAL MODEL OF ELECTROMAGNETIC COUPLING TO PIPELINE NETWORKS

Realistic pipelines may form a multi-branch interconnected network, and their interactions need to be considered. In addition, nonlinear polarization occurs between the metal and the soil at coating defects, which is also required to be included into the circuit of the pipe network. In this section, the nodal voltage analysis is used to evaluate the voltage and current responses of a pipeline network affected by EMI.

A. Equivalent-Pi Circuit for Linear Pipe Segments

The distributed TL model of each linear homogeneous pipe segment can be reduced to a lumped circuit with symmetric admittance parameters. Consider a pipeline with two terminal nodes i and k , which is excited by the external tangential electric field $E(x)$ as described in (12)-(13). For such an active two-port circuit, the relationship between the voltages and currents of the two ports can be reproduced by using an equivalent-pi circuit, where the effect of the external electric field is characterized by two lumped current sources at the ports, as shown in Fig. 4. The analytical solution of the parameters of the equivalent-pi circuit can be obtained by (16a)-(16d), and the derivation is detailed in our earlier work [12].

$$y_{ik} = \frac{1}{Z_C \sinh(\gamma L)} \quad (16a)$$

$$y_{ik0} = y_{ki0} = \frac{1}{Z_C} \tanh\left(\frac{\gamma L}{2}\right) \quad (16b)$$

$$j_{ik}^E = \frac{-1}{Z_C \sinh(\gamma L)} \int_0^L \cosh[\gamma(L-x)] E(x) dx \quad (16c)$$

$$j_{ki}^E = \frac{1}{Z_C \sinh(\gamma L)} \int_0^L \cosh(\gamma x) E(x) dx \quad (16d)$$

where $\gamma = \sqrt{ZY}$ is the propagation constant, $Z_C = \sqrt{Z/Y}$ is the characteristic impedance, and L is the length of the pipe.

Compared to the single-port Thévenin equivalent circuit [3], [9], the equivalent-pi circuit has the advantage that it can be performed for each single-conductor pipe individually according to its own TL parameters and tangential exciting electric field.

Moreover, the equivalent structure can be easily established in circuit simulation software for an intact pipeline, rather than manual segmentation of the distributed circuits [15]. If the pipeline is electrically short at the frequency of the incident field, a single lumped cell is adequate. Otherwise the usual options are (i) using the cascade connection of basic cells or (ii) relying on advanced macromodeling tools allowing to generate black-box behavioral models defined by mathematical relations [27].

In addition, it is also applicable to pipeline with some nonlinear grounded branches, e.g., on the coating defects. In this case, the pipeline can be simply divided into several segments at these defect nodes, and each segment can be reduced to an equivalent-pi circuit separately.

B. Nonlinear Polarization of Coating Breakdown

The insulation coating is added between the metal tube and the soil in the intact pipe segments. However, the coating may be damaged due to mechanical collision during the transport and burial process, as well as insulation aging.

The schematic diagram of the coating breakdown is depicted in Fig. 5(a). The damaged part is generally small, with a radius of several centimeters. Thus, each damaged part can be considered as a discrete node in the circuit [18]. For the breakdown node l , its influence on the pipe can be modeled as an additional grounded branch, as shown in Fig. 5(b), which includes contributions from the interface and the soil.

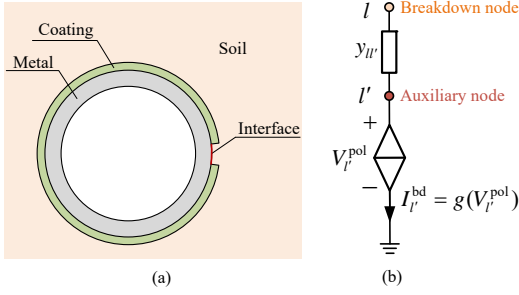


Fig. 5. Coating breakdown considering polarization effect at the interface. (a) Schematic diagram of the cross-section of the damaged part of the pipe; (b) Equivalent circuit of the breakdown node l , where $y_{ll'}$ is the linear soil conductance, $V_{l'}^{pol}$ is the polarization voltage, and $I_{l'}^{bd}$ is the leakage current.

At the interface where the coating is damaged, polarization effects occur due to the electrochemical reaction between the metal and the soil. An auxiliary node l' is added to describe it in the circuit. The potential difference across the interface, namely the polarization voltage $V_{l'}^{pol}$, is related to the leakage current density i^{leak} . Their relationship is usually nonlinear and can be obtained through electrochemical tests. For EMI calculation of pipelines, the piecewise interpolation method [19] or the Butler-Volmer model in (17) [20], [21], [24] can be used to fit the test data.

$$i^{leak} = i_0 \left[\exp\left(\frac{V_{l'}^{pol} - V_{corr}^{pol}}{\beta_a}\right) - \exp\left(-\frac{V_{l'}^{pol} - V_{corr}^{pol}}{\beta_c}\right) \right] \quad (17)$$

where the corrosion electrochemical parameters i_0 , V_{corr}^{pol} , β_a , β_c are the exchange current density, the natural corrosion potential, and the Tafel slope of the anode reaction and of the cathode reaction, respectively. They can be obtained by electrochemical tests. These parameters vary with the resistivity and pH value of the soil [21].

Assuming that the current is uniformly distributed at a breakdown node, then the polarization effect at the interface can be modeled as a nonlinear voltage-controlled current source. For instance, if the Butler-Volmer model is adopted, the leakage current $I_{l'}^{bd}$ of node l' can be determined by

$$\begin{aligned} I_{l'}^{bd} &= g(V_{l'}^{pol}) = S \cdot i^{leak} \\ &= S \cdot i_0 \left[\exp\left(\frac{V_{l'}^{pol} - V_{corr}^{pol}}{\beta_a}\right) - \exp\left(-\frac{V_{l'}^{pol} - V_{corr}^{pol}}{\beta_c}\right) \right] \end{aligned} \quad (18)$$

where S is the area of the damaged coating.

In addition, the linear admittance of the soil outside a defect depends on the soil parameters and the area of damaged part. It can be calculated by (19) for the analysis of DC or quasi-DC interference [18]. For higher frequency interference, more general equations for calculating the ground-return admittance can be found in [28]–[30].

$$y_{ll'} = \frac{4\sigma S}{4d + \sqrt{\pi S}} \quad (19)$$

where σ is the soil conductivity and d is the coating thickness.

C. Nodal Voltage Analysis of the Pipeline Network

The nodal voltage analysis is performed for the electromagnetic coupling analysis of the pipeline network, which contains

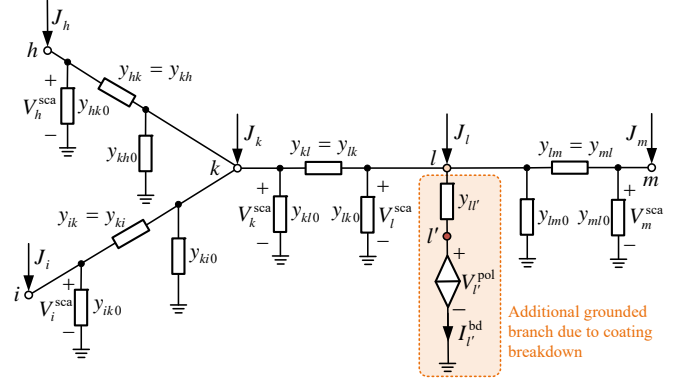


Fig. 6. Schematic diagram of the circuit model of an illustrative pipeline network considering nonlinear polarization at breakdown node l .

linear pipe segments and coating breakdown with nonlinear polarization. As for node sets, \mathcal{N}_{nml} is the set of normal nodes, including terminals, bends, and junctions, \mathcal{N}_{bd} is the set of breakdown nodes, and \mathcal{N}'_{bd} is the set of auxiliary breakdown nodes. The cardinal numbers of these node sets are denoted as $n_1 = |\mathcal{N}_{nml}|$ and $n_2 = |\mathcal{N}_{bd}| = |\mathcal{N}'_{bd}|$. Thus, the set of full nodes in the network is denoted as $\mathcal{N} = \mathcal{N}_{nml} \cup \mathcal{N}_{bd} \cup \mathcal{N}'_{bd}$, and the total number of nodes is $n = n_1 + 2n_2$.

A demonstrative example of the pipeline network is depicted in Fig. 6. The original pipeline network consists of four normal nodes $\{h, i, k, m\}$ and three pipes $\{(h, k), (i, k), (k, m)\}$. Assume there exists a breakdown point l on the pipe (k, m) , then the pipe can be divided into two segments (k, l) and (l, m) . Meanwhile, an additional grounded branch, including an auxiliary node l' , is added at node l .

The equivalent- π circuit can be established for each pipe segment according to (16a)–(16d). The current sources in the equivalent- π circuit of each segment due to the external electric fields are integrated in the $(n_1 + n_2) \times 1$ nodal current injection vector \mathbf{J} for the node sets \mathcal{N}_{nml} and \mathcal{N}_{bd} as

$$J_i = \sum_{k \in N(i)} j_{ik}^E \quad (20)$$

where $N(i)$ the set of all neighboring nodes that are directly connected to node i .

Then the voltage equation can be formulated for each node. For the normal node $i \in \mathcal{N}_{nml}$, according to Kirchhoff's current law, we can obtain

$$\sum_{k \in N(i)} [y_{ik}(V_i^{sca} - V_k^{sca}) + y_{ik0}V_i^{sca}] = J_i \quad (21)$$

Similarly, for the breakdown node $l \in \mathcal{N}_{bd}$, one can get

$$\begin{aligned} \sum_{k \in N(l), k \neq l'} [y_{lk}(V_l^{sca} - V_k^{sca}) + y_{lk0}V_l^{sca}] \\ + y_{ll'}(V_l^{sca} - V_{l'}^{pol}) = J_l \end{aligned} \quad (22)$$

For the auxiliary node $l' \in \mathcal{N}'_{bd}$, one can get

$$y_{ll'}(V_l^{sca} - V_{l'}^{pol}) = I_{l'}^{bd} = g(V_{l'}^{pol}) \quad (23)$$

The variables to be solved include the $(n_1 + n_2) \times 1$ scattered voltages \mathbf{V}^{sca} and the $n_2 \times 1$ polarization voltages \mathbf{V}^{pol} . They

can be collectively denoted as the $n \times 1$ full-node voltages $\tilde{\mathbf{V}}$. To sum up, the voltage equations (21)-(23) for all n nodes can be expressed in a compact matrix form with respect to $\tilde{\mathbf{V}}$:

$$\mathbf{f}(\tilde{\mathbf{V}}) := \mathbf{Y}^{\text{init}}\tilde{\mathbf{V}} + \begin{bmatrix} -\mathbf{J} \\ \mathbf{I}^{\text{bd}} \end{bmatrix} = \mathbf{0}, \quad \text{where } \tilde{\mathbf{V}} = \begin{bmatrix} \mathbf{V}^{\text{sca}} \\ \mathbf{V}^{\text{pol}} \end{bmatrix} \quad (24)$$

\mathbf{Y}^{init} is the $n \times n$ initial admittance matrix ignoring the grounded branch of the auxiliary breakdown nodes \mathcal{N}'_{bd} . The diagonal entries of \mathbf{Y}^{init} , which depend on the node type, are given as

$$Y_{ii}^{\text{init}} = \sum_{k \in N(i)} (y_{ik} + y_{ik0}), \quad \text{if } i \in \mathcal{N}_{\text{nmI}} \quad (25)$$

$$Y_{ll}^{\text{init}} = y_{ll'} + \sum_{k \in N(l), k \neq l'} (y_{lk} + y_{lk0}), \quad \text{if } l \in \mathcal{N}_{\text{bd}} \quad (26)$$

$$Y_{l'l'}^{\text{init}} = y_{l'l'}, \quad \text{if } l' \in \mathcal{N}'_{\text{bd}} \quad (27)$$

and the off-diagonal entries are given as

$$Y_{ik}^{\text{init}} = \begin{cases} -y_{ik}, & \text{if } k \in N(i) \wedge k \neq i \\ 0, & \text{if } k \notin N(i) \wedge k \neq i \end{cases} \quad (28)$$

\mathbf{I}^{bd} is the $n_2 \times 1$ earthing current of the node set \mathcal{N}'_{bd} , and its l' -th entry $I_{l'}^{\text{bd}}$ depends on the polarization voltage $V_{l'}^{\text{pol}}$ as in (18).

D. Solving Nodal Voltages via Newton-Raphson Method

The nodal voltage equation (24) has no closed-form solution in the presence of the nonlinear term \mathbf{I}^{bd} . Such a set of nonlinear algebraic equations can be solved by numerical methods such as Newton-Raphson iteration [31]. The nodal voltages $\tilde{\mathbf{V}}$ iterates from the initial guess and gradually converges to the exact solution.

One possible method to determine the initial guess of the nodal voltages $\tilde{\mathbf{V}}^{(0)}$ is by neglecting the leakage currents at the breakdown nodes as in (29). Alternatively, a different initial guess of nodal voltages can be obtained by replacing the controlled voltage source with other linear admittance.

$$\mathbf{Y}^{\text{init}}\tilde{\mathbf{V}}^{(0)} = \begin{bmatrix} \mathbf{J} \\ \mathbf{0} \end{bmatrix} \quad (29)$$

where $\mathbf{0}$ is a $n_2 \times 1$ zero vector.

Then, the nodal voltages can then be continuously corrected according to the mismatch in (24). At step k , the nodal voltages iterates in the following format:

$$\left. \begin{aligned} \mathbf{Y}^{(k)} \Delta \tilde{\mathbf{V}}^{(k)} &= -\mathbf{f}(\tilde{\mathbf{V}}^{(k)}) \\ \tilde{\mathbf{V}}^{(k+1)} &= \tilde{\mathbf{V}}^{(k)} + \Delta \tilde{\mathbf{V}}^{(k)} \end{aligned} \right\} (k = 0, 1, 2, \dots) \quad (30)$$

where \mathbf{Y} is the $n \times n$ Jacobian matrix, which consists of the first-order partial derivatives of the functions in (24) with respect to the nodal voltages:

$$\mathbf{Y} := \frac{\partial \mathbf{f}(\tilde{\mathbf{V}})}{\partial \tilde{\mathbf{V}}} \quad (31)$$

It can be found that the Jacobian matrix \mathbf{Y} is actually the nodal admittance matrix containing the dynamic conductance of the grounded branch of the auxiliary breakdown nodes. Thus, the Jacobian matrix $\mathbf{Y}^{(k)}$ at the k -th iteration can be

obtained by small corrections to the initial admittance matrix \mathbf{Y}^{init} : the diagonal entries corresponding to the auxiliary nodes \mathcal{N}'_{bd} needs be updated as in (32) if the Butler-Volmer equation (17) is used to characterized the polarization effect, whereas other entries in the matrix remain unchanged.

$$\begin{aligned} Y_{l'l'}^{(k)} &= Y_{l'l'}^{\text{init}} + \left. \frac{dg(\tilde{V}_{l'})}{d\tilde{V}_{l'}} \right|_{\tilde{V}_{l'} = \tilde{V}_{l'}^{(k)}} \\ &= Y_{l'l'}^{\text{init}} + S \cdot i_0 \left[\frac{1}{\beta_a} \exp\left(\frac{\tilde{V}_{l'}^{(k)} - V_{\text{corr}}^{\text{pol}}}{\beta_a}\right) \right. \\ &\quad \left. + \frac{1}{\beta_c} \exp\left(-\frac{\tilde{V}_{l'}^{(k)} - V_{\text{corr}}^{\text{pol}}}{\beta_c}\right) \right], \quad \forall l' \in \mathcal{N}'_{\text{bd}} \end{aligned} \quad (32)$$

The nodal voltages are considered to have converged if the following criterion is satisfied:

$$\|\mathbf{f}(\tilde{\mathbf{V}}^{(k)})\|_{\infty} = \max_i |f_i(\tilde{\mathbf{V}}^{(k)})| < \varepsilon \quad (33)$$

where ε is the tolerance error of the mismatch.

E. Voltages and Currents Along Intact Pipe Segments

Once the nodal scattered voltages are obtained, we can further calculate the responses along the pipeline of interest. The voltages and currents along the pipe (i, k) can be solved from the terminal voltages V_i^{sca} and V_k^{sca} :

$$I(x) = [A + P(x)]e^{-\gamma x} + [B + Q(x)]e^{\gamma x} \quad (34)$$

$$V^{\text{sca}}(x) = Z_C \{ [A + P(x)]e^{-\gamma x} - [B + Q(x)]e^{\gamma x} \} \quad (35)$$

where

$$A = \frac{y_{ik}}{2}(V_i^{\text{sca}}e^{\gamma L} - V_k^{\text{sca}}) - \frac{j_{ik}^E}{2} \quad (36a)$$

$$B = \frac{y_{ik}}{2}(V_i^{\text{sca}}e^{-\gamma L} - V_k^{\text{sca}}) + \frac{j_{ki}^E}{2}e^{-\gamma L} \quad (36b)$$

$$P(x) = \frac{1}{2Z_C} \int_0^x e^{\gamma \xi} E(\xi) d\xi \quad (36c)$$

$$Q(x) = \frac{1}{2Z_C} \int_x^L e^{-\gamma \xi} E(\xi) d\xi \quad (36d)$$

where y_{ik} , j_{ik}^E and j_{ki}^E are the parameters of the equivalent-pi circuit for pipe (i, k) in Section III-A.

F. Procedure for EMI Calculation of Pipeline Network

The procedures for calculating the electromagnetic coupling to the pipeline network are summarized in Algorithm 1. Some preprocessing is required to obtain the inputs before starting the algorithm. Firstly, the spatial distribution of the external exciting electric field needs to be simulated by using the source currents and earth resistivity structure, etc [12], [13]. Secondly, the breakdown nodes and auxiliary nodes are added for each pipeline, which can be determined by coating defect detector [18] or related engineering experience [21]. Thus, it yields a new graph $\mathcal{G} = (\mathcal{N}, \mathcal{E})$ for the pipe network, where \mathcal{N} is a set of full nodes and \mathcal{E} is a set of all pipe segments.

Algorithm 1: Electromagnetic Coupling to Pipeline Networks Considering Nonlinear Polarization Effects

Data: A pipeline network $\mathcal{G} = (\mathcal{N}, \mathcal{E})$ with topology and nodal coordinates; TL parameters of each pipeline; polarization characteristics of coating breakdown; spatial distribution of exciting electric field; tolerable error ε and maximum iteration N_{iter} for Newton-Raphson method.

Result: PSPs and currents along the pipes of interest.

```

1 for  $(i, k)$  in  $\mathcal{E}$  do
2   Calculate the parameters of equivalent-pi circuit for
   pipeline  $(i, k)$  using (16a)-(16d);
3 end
4 Make the nodal current injection vector  $\mathbf{J}$  via (20) and
   initial network admittance matrix  $\mathbf{Y}^{\text{init}}$  via (25)-(28);
5 Obtain the initial guess of full-node voltages  $\tilde{\mathbf{V}}^{(0)}$  in
   the pipeline network by solving (29);
6 Initialize counter  $k \leftarrow 0$  for Newton-Raphson iteration;
7 repeat
8   Initialize the Jacobian matrix  $\mathbf{Y}^{(k)} \leftarrow \mathbf{Y}^{\text{init}}$ ;
9   for  $l'$  in  $\mathcal{N}'_{\text{bd}}$  do
10    Update  $Y_{l'l'}^{(k)}$  using  $\tilde{V}_{l'}^{(k)}$  as in (32);
11  end
12  Calculate the updated voltages  $\tilde{\mathbf{V}}^{(k+1)}$  via (30);
13  Increment iteration counter step  $k \leftarrow k + 1$ ;
14  if  $k \geq N_{\text{iter}}$  then
15    The Newton-Raphson algorithm does not
    converge. Re-select the initial guess of nodal
    voltages  $\tilde{\mathbf{V}}^{(0)}$  and goto line 6;
16  end
17 until  $\|\mathbf{f}(\tilde{\mathbf{V}}^{(k)})\|_{\infty} < \varepsilon$ ;
18 Extract  $\mathbf{V}^{\text{sca}}$  and  $\mathbf{V}^{\text{pol}}$  from  $\tilde{\mathbf{V}}^{(k)}$ ;
19 for  $(i, k)$  in  $\mathcal{E}$  do
20   Calculate the longitudinal currents and scattered
   voltages along the intact pipe segment  $(i, k)$  using
    $V_i^{\text{sca}}$  and  $V_k^{\text{sca}}$  as in (34)-(35);
21   Calculate the leakage current density and PSP
   along the pipe  $(i, k)$  using the scattered voltages
   via (14)-(15);
22 end
23 for  $l'$  in  $\mathcal{N}'_{\text{bd}}$  do
24   Calculate the leakage current density at the
   breakdown node  $l'$  using  $V_{l'}^{\text{pol}}$  as in (17);
25 end
  
```

IV. MODEL VALIDATION

The proposed equivalence method for pipelines has been verified in [12] in the case of inductive EMI caused by geomagnetic disturbances. This paper further illustrates its validity for conductive coupling analysis.

The authors of [17] carried out a field test of the interference of DC current sources on a short buried pipeline, as depicted in Fig. 7. The length of the pipeline is 39.3 m, and the buried depth is 0.8 m. The outer diameter of the steel tube is 200 mm, and its wall thickness is 5 mm. The steel resistivity is $1.75 \times$

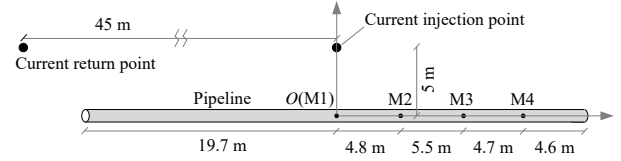


Fig. 7. Schematic diagram of the field test of a short pipeline [17].

TABLE I
TWO-LAYER HORIZONTAL SOIL RESISTIVITY STRUCTURE [17]

Layer	Resistivity ($\Omega \cdot \text{m}$)	Thickness (m)
1	31	2.5
2	79	∞

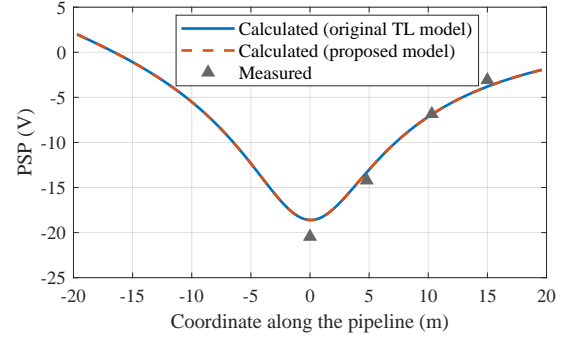


Fig. 8. Comparison of calculated and measured PSPs along the pipeline.

$10^{-7} \Omega \cdot \text{m}$. The steel tube is wrapped with 3PE insulation coating. Its thickness is 3 mm and its resistivity is $3.33 \times 10^7 \Omega \cdot \text{m}$. The insulation coating is intact along the pipe. The left and right ends of the pipe were respectively connected to a vertical grounding rod with a length of 1.5 m and a diameter of 10 mm. Four potential measurement points were arranged along the pipe, including M1, M2, M3 and M4. The point M1 was taken as the origin. The 1D layered soil resistivity structure, as shown in Table I, was measured by the Wenner method.

The PSPs along the pipeline are calculated using the proposed model and the classical model, which are compared with the measured data, as depicted in Fig. 8. It is worth noting that in this paper, PSP is defined by subtracting the outer soil potential from the inner metal potential of the coating, whereas [17] takes the opposite reference direction. Besides, the slight asymmetry of potential distribution along the pipeline is affected by the current return point. In the proposed model, the pipeline is reduced to an equivalent-pi circuit. Thus, the voltage response can be solved based on a two-node admittance matrix. In contrast, in the classical model, the pipeline is discretized based on the original TL equations (3)-(4). Hence, the proposed method enables a considerable reduction in model size, as shown in Table II. The results of the two computational models are highly consistent, and they both agree well with the test data, which validates the accuracy of the proposed method.

TABLE II
COMPUTATIONAL PERFORMANCE OF THE CLASSICAL
DISCRETIZATION METHOD AND THE PROPOSED EQUIVALENCE
METHOD FOR THE VALIDATION CASE

Number of segments	Size of the coefficient matrix		Memory of the sparse coefficient matrix (kB)	
	Classical	Proposed	Classical	Proposed
500	501×501	2×2	27.38	0.0859
1000	1001×1001	2×2	54.72	0.0859
2000	2001×2001	2×2	109.41	0.0859

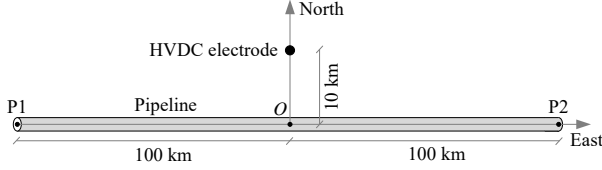


Fig. 9. Schematic diagram of a simulation case including a long pipeline and a HVDC grounding electrode.

V. APPLICATION STUDY

In this section, the proposed computational model is applied to the EMI analysis of long pipelines and interconnected networks. First we analyze the response of a pipeline to typical conductive and inductive interference, including HVDC earth return currents and geomagnetic disturbances. We then analyze the influence of the coating breakdown and illustrate the significance of the polarization effects.

A. Response of the Intact Pipeline to HVDC Earth Return Currents and Geomagnetic Disturbances

Let us consider a more realistic 200 km pipeline as shown in Fig. 9. The outer diameter of the steel tube is 1016 mm, and its wall thickness is 12 mm [20]. The steel resistivity is $1.75 \times 10^{-7} \Omega \cdot \text{m}$. The coating has a thickness of 3 mm and a resistivity of $3.33 \times 10^7 \Omega \cdot \text{m}$. In this subsection, the coating is assumed to be intact. The pipeline is buried in a $100 \Omega \cdot \text{m}$ homogeneous earth at a depth of 1.5 m. A discussion on the response of pipelines in spatially heterogeneous soils can be found in [12].

The first type interference is caused by a nearby HVDC grounding electrode. The electrode is 10 km away from the midpoint of the pipeline. Its buried depth is 3 m, and the earthing current is -5 kA. The resulting excitation voltage and tangential exciting electric field along the pipeline are shown in Fig. 10. It can be seen that the excitation voltage has a peak value of -7.96 V at the center of the pipe and that the tangential electric field reaches a peak of 0.31 V/km at a distance of 7.1 km from the midpoint. The second type interference is geomagnetic disturbances, which correspond to a uniform 0.1 V/km eastward geoelectric field. The pipeline response to the two types of disturbances is then calculated separately. The above is the default simulation configuration in this section unless otherwise specified.

Fig. 11 compares the PSP, leakage current density, and longitudinal current along the pipe in the two interference cases. In the case of interference from the HVDC grounding electrode, the peak value of PSP is 5.16 V, which appears

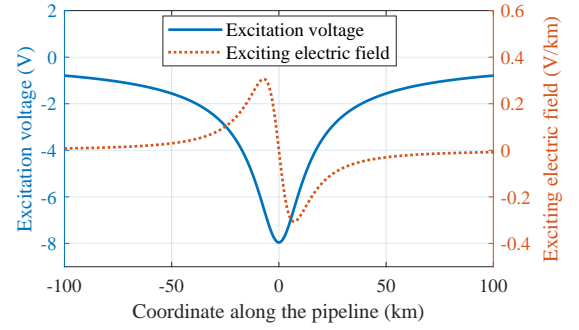


Fig. 10. The excitation voltage and tangential exciting electric field along the pipeline caused by the HVDC earth return currents.

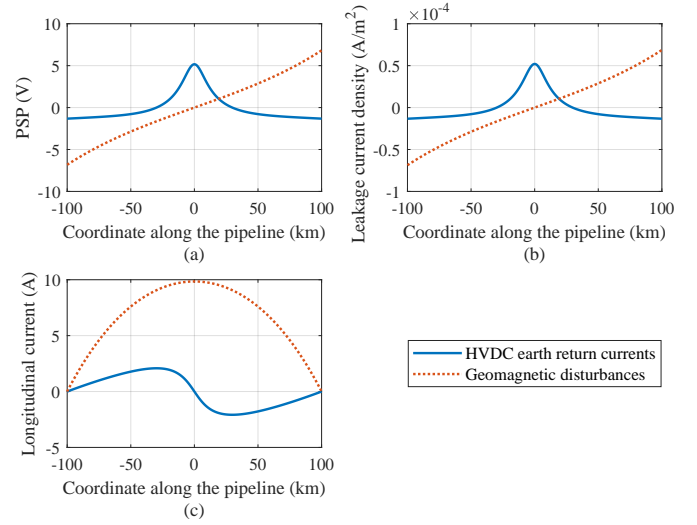


Fig. 11. Pipeline response to HVDC earth return currents and geomagnetic disturbances. (a) PSP. (b) Leakage current density. (c) Longitudinal current.

at the midpoint of the pipeline. In the case of geomagnetic disturbances, the peak value of PSP amplitude is 6.82 V, which appears at the two ends of the pipe. The leakage current density along the pipe is proportional to the PSP, and its peak values in the two interference cases are $5.20 \times 10^{-5} \text{ A/m}^2$ and $6.87 \times 10^{-5} \text{ A/m}^2$, respectively. The peak of the longitudinal current is located at the zero crossing point of the PSP.

B. Influence of Nonlinear Polarization Effect

The influence of coating breakdown is analyzed in this subsection. The damage points are assumed to be equally spaced at an interval of 10 km. The area of the damaged coating of each node is 5 cm^2 . Based on the electrochemical test data for the $100 \Omega \cdot \text{m}$ soil, the fitted Butler-Volmer polarization equation is given by [20]

$$i = 3.66 \times \left[\exp\left(\frac{V_{l'}^{\text{pol}} + 0.304}{2.45}\right) - \exp\left(-\frac{V_{l'}^{\text{pol}} + 0.304}{4.94}\right) \right] \quad (37)$$

The corresponding nonlinear polarization curve is shown in Fig. 12. When the leakage current density is zero, the interface of the coating defect works at the natural corrosion potential -0.304 V. When the leakage current density is in the range

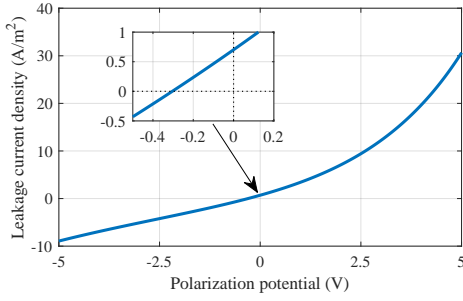


Fig. 12. Polarization curve of the pipe steel in $100 \Omega \cdot \text{m}$ soil.

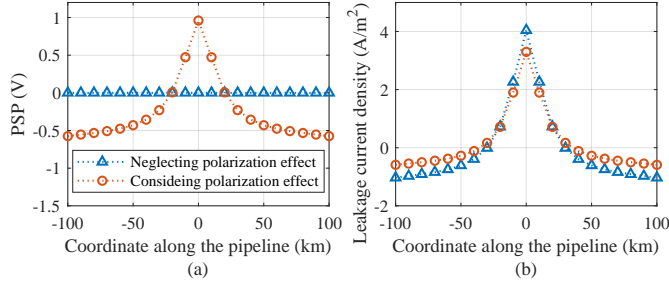


Fig. 13. Response of the coating defects due to HVDC earth return currents. (a) PSP of the interface. (b) Leakage current density.

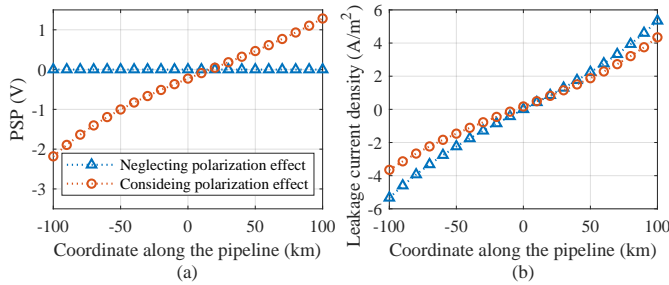


Fig. 14. Response of the coating defects due to geomagnetic disturbances. (a) PSP of the interface. (b) Leakage current density.

of $0 \sim 0.702 \text{ A/m}^2$, the polarization curve is in the second quadrant, which means it behaves as a negative resistance.

Then, we calculate the polarization voltage and leakage current density of the coating defects using two calculation models. In the first model, the polarization effect at the damaged interface is neglected, and only the external soil resistance is considered [11]. In the second model, however, both effects are considered.

The response of the coating defects to the HVDC earth return currents and geomagnetic disturbances are shown in Fig. 13 and Fig. 14, respectively. If the polarization effect is neglected, the PSPs at the interface of the damaged coating are considered to be zero. In addition, the leakage current density of the coating defects at the midpoint of the pipe is overestimated by 22.6% for the HVDC interference; and the leakage current densities at the left and right ends are overestimated by 46.3% and 22.9% for the geomagnetic disturbances, respectively. Moreover, the magnitude of the leakage current density of the coating defects is much higher than that of the intact coating in Fig. 11(b).

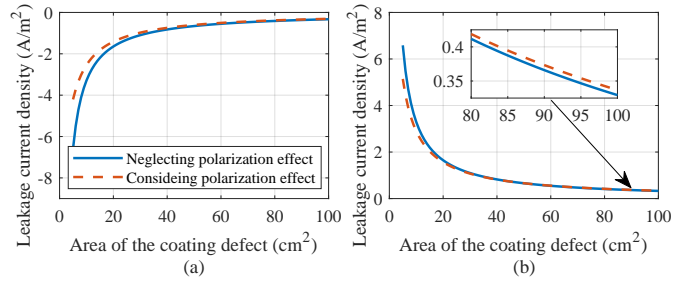


Fig. 15. Leakage current density induced by geomagnetic disturbances with respect to the area of the coating defect. (a) Left end of the pipe. (b) Right end of the pipe.

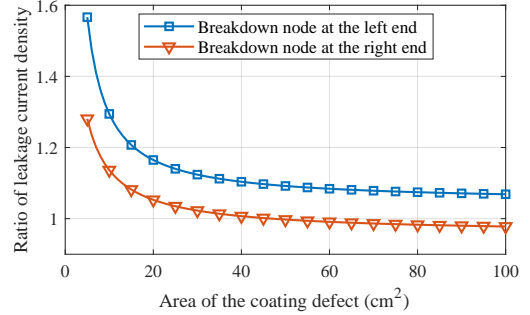


Fig. 16. Ratio of the leakage current density induced by geomagnetic disturbances neglecting and considering the polarization effect with respect to the area of coating defect.

C. Influence of the Area of Coating Defect

We then discuss the influence of the area of damaged coating. The area of each coating defect ranges from 5 cm^2 to 100 cm^2 . The total number and distance of the defects are the same as in the previous subsection. Fig. 15 shows the leakage current density of the coating defects at the left and right ends of the pipe due to geomagnetic disturbances. As the damaged area increases, the leakage current density at both ends decreases gradually.

In order to indicate the contribution of the polarization effect more clearly, we further adopt a normalized metric, i.e. the ratio of the leakage current density of the coating defects without and with consideration of the polarization effect. Fig. 16 depicts the variation of this ratio with respect to the area of coating defects. It can be seen that the ratio of leakage current density at the left and right ends decreases with the increase of the damaged area and that the polarization effect has a stronger influence on the current leakage density of the left end than that of the right end. Moreover, for the coating defects at the right end, the ratio may be less than 1 when the damaged area is large, since it works in second quadrant in Fig. 12 in this case.

D. A Pipeline Network Test Case

Next, the applicability of the proposed method is illustrated with an interconnected pipeline network with nine nodes and eight lines, as depicted in Fig. 17. The TL parameters and nodal coordinates of the pipeline network can be found in [10], [12]. The network contains a main pipeline “3-4-5-6-7-

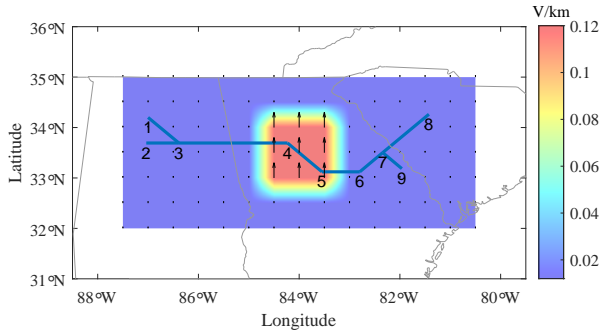


Fig. 17. Spatial distribution of pipeline networks [10], [12] and nonuniform geoelectric fields [32]. The black arrows show the direction and magnitude of the geoelectric field. The black number is the node index in the pipeline network.

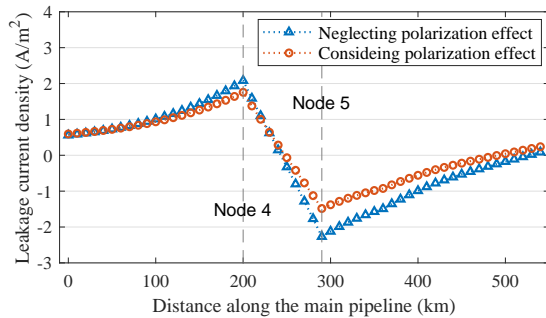


Fig. 18. Leakage current density of the coating defects along the main pipeline.

8” and three branch lines “1-3”, “2-3” and “7-9”. The coating defects are assumed to be equally spaced at an interval of 10 km on each pipeline. The area of each defect is 5 cm². The external nonuniform geoelectric field is caused by the spatially local enhancement of the geomagnetic variations. The electric field data are provided in report [32] with a 0.5° × 0.5° grid, and the values in this paper are scaled to 1% of the original as a representative level of more frequent moderate and small geomagnetic disturbances. A finer spatial distribution of the electric field is obtained by linear interpolation.

Fig. 18 shows the leakage current density along the main pipeline. It can be seen that the amplitude of the leakage current density reaches the extreme value at nodes 4 and 5. Ignoring the polarization effect leads to an overestimation of the leakage current density by 18.5% and 52.8% at nodes 4 and 5, respectively.

Finally, the computational performance of the classical discretization method and the proposed equivalence method is compared using a historical geomagnetic disturbance event. The geomagnetic data with 1-minute time cadence measured at Beijing Ming Tombs (BMT) observatory during the event on July 15-16, 2000 [13] are used as inputs, and the corresponding number of time instants is 2880. In the classical method, the pipe between two adjacent coating defects is divided into 100 segments. The algorithms are tested using MATLAB R2019b software on a desktop with a 3.0 GHz Intel i7-9700 CPU and 8 GB RAM. Table III provides the details of these two calculation methods, including the size of the system of equations,

TABLE III
COMPUTATIONAL PERFORMANCE OF THE CLASSICAL DISCRETIZATION METHOD AND THE PROPOSED EQUIVALENCE METHOD FOR THE PIPELINE NETWORK TEST CASE

Calculation methods	Size of the coefficient matrix	Memory of the sparse coefficient matrix (kB)	Computation times (s)
Classical	7375×7375	404.44	132.24
Proposed	148×148	9.21	4.51

memory requirements and computation times. It shows that the proposed equivalence method can improve computational performance, especially when fine discretization is required to capture the complex spatial nonuniform distribution of the exciting electric field.

VI. CONCLUSION AND FUTURE WORK

This paper proposes a generalized modeling and equivalence technique for the analysis of EMI on pipeline networks due to nonuniform fields. The computational model is reduced through the equivalent- π circuit. The proposed method is validated by comparison with the classical discretization method and field tests. Based on the proposed model, we compare the response of buried pipelines to HVDC earth return currents and geomagnetic disturbances. In addition, the influence of the coating breakdown and the polarization effect are analyzed. The results show that when the damaged area is small, the leakage current density is relatively large and the influence of the polarization effect is strong, which needs to be considered in the corrosion assessment for pipelines.

The proposed method can be extended to other EMI analysis of pipelines. It can also significantly reduce the computational burden and help in the optimization of mitigation measures, where a large number of different configurations need to be analyzed. Further work is in progress to establish an improved equivalent circuit model for multi-conductor pipelines.

APPENDIX A

PROOF OF THE MODIFIED TL CIRCUIT IN FIG. 2

For the top panel of Fig. 2, we can obtain the two-port representation of the original TL circuit model:

$$I(x) = [V(x) - V(x + dx)] \frac{1}{Z dx} \quad (38)$$

$$I(x + dx) = I(x) - [V(x + dx) - V^{\text{exc}}(x + dx)] \cdot Y dx \quad (39)$$

The scattered voltage is defined as the difference between the voltage of the metal side to the remote earth and the excitation voltage of the nearby soil:

$$V^{\text{sca}}(x) := V(x) - V^{\text{exc}}(x) \quad (40)$$

$$V^{\text{sca}}(x + dx) := V(x + dx) - V^{\text{exc}}(x + dx) \quad (41)$$

Substituting equations (40)-(41) into (38)-(39), the two-port representation can be rewritten as

$$I(x) = [V^{\text{sca}}(x) - V^{\text{sca}}(x + dx)] \frac{1}{Z dx} + [V^{\text{exc}}(x) - V^{\text{exc}}(x + dx)] \frac{1}{Z dx} \quad (42)$$

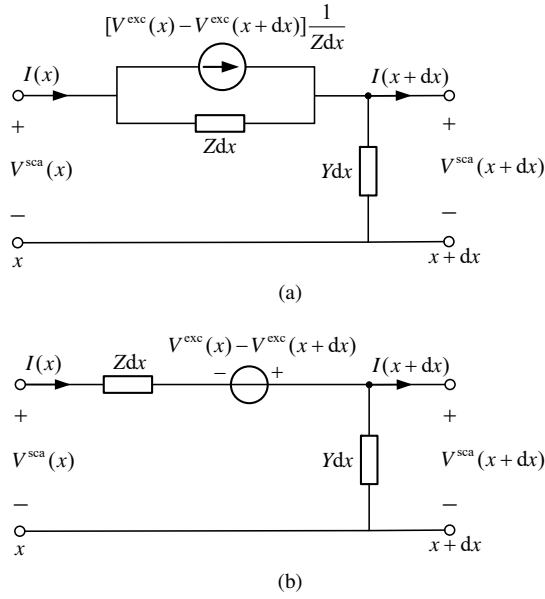


Fig. 19. Modified circuit models of a pipeline affected by the conductive interference. (a) Current source interpretation. (b) Voltage source interpretation.

$$I(x+dx) = I(x) - V^{\text{sca}}(x+dx) \cdot Ydx \quad (43)$$

The circuit interpretation of equations (42)-(43) is depicted in Fig. 19(a), where an equivalent current source is added to the longitudinal branch of the modified structure. Then, by converting from Norton to Thévenin equivalent circuit, we can obtain the voltage source representation as shown in Fig. 19(b).

Using the approximation of a difference operator

$$E^{\text{con}}(x) := -\frac{dV^{\text{exc}}(x)}{dx} = -\frac{V^{\text{exc}}(x+dx) - V^{\text{exc}}(x)}{dx} \quad (44)$$

the voltage source can be rewritten as

$$V^{\text{exc}}(x) - V^{\text{exc}}(x+dx) = E^{\text{con}}(x)dx \quad (45)$$

In summary, the top panel of Fig. 2 can be interpreted as the equivalent circuit in the bottom panel of Fig. 2.

APPENDIX B

PROOF OF THE MODIFIED TL CIRCUIT IN FIG. 3

Similarly, for the top panel of Fig. 3, we can obtain the two-port representation of the original TL circuit model

$$I(x) = [V(x) - V(x+dx) + E^{\text{ind}}(x)dx] \frac{1}{Zdx} \quad (46)$$

$$I(x+dx) = I(x) - [V(x+dx) - V^{\text{exc}}(x+dx)] \cdot Ydx \quad (47)$$

Substituting equations (40)-(41) into (46)-(47), the two-port representation can be rewritten as

$$I(x) = [V^{\text{sca}}(x) - V^{\text{sca}}(x+dx)] \frac{1}{Zdx} + [E^{\text{ind}}(x)dx + V^{\text{exc}}(x) - V^{\text{exc}}(x+dx)] \frac{1}{Zdx} \quad (48)$$

$$I(x+dx) = I(x) - V^{\text{sca}}(x+dx) \cdot Ydx \quad (49)$$

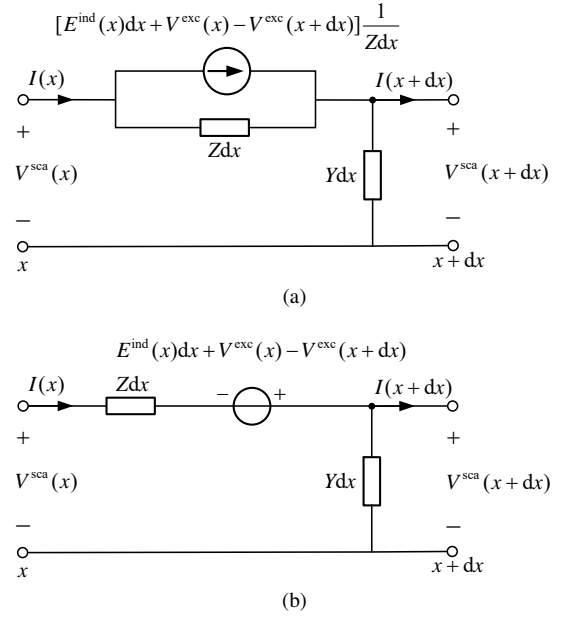


Fig. 20. Modified circuit models of a pipeline affected by both inductive and conductive interference. (a) Current source interpretation. (b) Voltage source interpretation.

The circuit interpretation of equations (48)-(49) is depicted in Fig. 20(a), where an equivalent current source is added to the longitudinal branch, which can be further converted into the voltage source representation shown in Fig. 20(b).

Given the total exciting electrical field tangential to the pipeline

$$\begin{aligned} E(x) &:= E^{\text{ind}}(x) + E^{\text{con}}(x) = E^{\text{ind}}(x) - \frac{dV^{\text{exc}}(x)}{dx} \\ &= E^{\text{ind}}(x) - \frac{V^{\text{exc}}(x+dx) - V^{\text{exc}}(x)}{dx} \end{aligned} \quad (50)$$

the voltage source can be rewritten as

$$E^{\text{ind}}(x)dx + V^{\text{exc}}(x) - V^{\text{exc}}(x+dx) = E(x)dx \quad (51)$$

To summarize, the top panel of Fig. 3 can be interpreted as the equivalent circuit in the bottom panel of Fig. 3.

APPENDIX C

HANDLING ADDITIONAL GROUNDED BRANCHES

The pipe node may be connected to the grounded in engineering practice. Assuming an additional grounded branch connects the pipeline node k to the grounded. Let us denote the voltage of the metal side of pipe node k to the remote earth as V_k , and the soil potential rise near node k as V_k^{exc} . The soil potential rise of the grounded is V_k^{gnd} . The grounding impedance of node k is Z_k , and the grounding current is I_k^{gnd} .

For the original circuit model of the grounded branch at node k as depicted in Fig. 21(a), the voltage of the metal side of pipe node k to the remote earth can be written as

$$V_k = I_k^{\text{gnd}} Z_k + V_k^{\text{gnd}} \quad (52)$$

Thus, the scattered voltage of node k can be derived as

$$V_k^{\text{sca}} := V_k - V_k^{\text{exc}} = I_k^{\text{gnd}} Z_k + (V_k^{\text{gnd}} - V_k^{\text{exc}}) \quad (53)$$

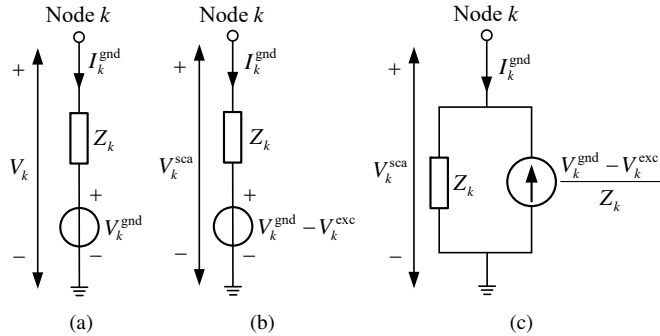


Fig. 21. Circuit models of the additional grounded branch of a pipe node. (a) Original circuit. (b) Modified circuit using the voltage source interpretation. (c) Modified circuit using the current source interpretation.

The circuit interpretation of equation (53) is depicted in Fig. 21(b), where a voltage source is added to characterize the difference in the excitation voltage between the pipe and the groundbed. It can be further converted into a current source shown in Fig. 21(c) with Norton equivalent system, which can be easily incorporated into the nodal current injection vector in (20). Especially, if the pipe node k is close to the groundbed, i.e. their soil potential rises are approximately equal ($V_k^{\text{exc}} \approx V_k^{\text{gnd}}$), then the additional current source is zero.

ACKNOWLEDGMENT

The authors would like to thank Fangyuan Cao from China Electric Power Research Institute and Dr. David Boteler from Natural Resources Canada for their valuable comments on the article. For the geomagnetic data at BMT observatory used in this paper, the authors gratefully acknowledge the SuperMAG ground magnetometer data released for the public (<http://supermag.jhuapl.edu/info/?page=acknowledgement>).

REFERENCES

- [1] L. Coelho, G. Sotelo, and A. C. Lima, "Detailed versus simplified representation of a pipeline for assessment of inductive and conductive couplings to an overhead transmission lines during steady-state and fault conditions," *Int. J. Electr. Power Energy Syst.*, vol. 142, 2022, Art. no. 108350.
- [2] D. Rabah, M. Lahdeb, S. Ghoneim, and D. Mahi, "Combined effects of electrostatic and electromagnetic interferences of high voltage overhead power lines on aerial metallic pipeline," *Facta Univ. - Ser. Electron. Energ.*, vol. 35, no. 3, pp. 349–377, 2022.
- [3] A. Taflove and J. Dabkowski, "Prediction method for buried pipeline voltages due to 60 Hz AC inductive coupling part I-analysis," *IEEE Trans. Power App. Syst.*, vol. PAS-98, no. 3, pp. 780–787, 1979.
- [4] F. Dawalibi and R. Southey, "Analysis of electrical interference from power lines to gas pipelines. II. parametric analysis," *IEEE Trans. Power Del.*, vol. 5, no. 1, pp. 415–421, 1990.
- [5] G. Lucca, "Electromagnetic interference from power lines on pipelines: influence of pipe insulating coating degradation," *Int. Trans. Electr. Energy Syst.*, vol. 26, no. 12, pp. 2699–2712, 2016.
- [6] C. Wang, X. Liang, and R. Radons, "Minimum separation distance between transmission lines and underground pipelines for inductive interference mitigation," *IEEE Trans. Power Del.*, vol. 35, no. 3, pp. 1299–1309, 2020.
- [7] D. Boteler, C. A. Charalambous, and K. Lax, "New insights into calculations of AC interference at fundamental and harmonic frequencies taking account of the phase relationships of the currents," *IEEE Trans. Power Del.*, vol. 37, no. 2, pp. 851–859, 2022.
- [8] D. Boteler and M. Cookson, "Telluric currents and their effects on pipelines in the cook strait region of New-Zealand," *Mater. Perform.*, vol. 25, no. 3, pp. 27–32, 1986.
- [9] A. Pulkkinen, R. Pirjola, D. Boteler, A. Viljanen, and I. Yegorov, "Modelling of space weather effects on pipelines," *J. Appl. Geophys.*, vol. 48, no. 4, pp. 233–256, 2001.
- [10] D. Boteler, "A new versatile method for modelling geomagnetic induction in pipelines," *Geophys. J. Int.*, vol. 193, no. 1, pp. 98–109, 2013.
- [11] C. Ma and C. Liu, "Influence of pipeline insulation leakage points on the distribution of geomagnetically induced current and pipe-soil potential," *IEEE Access*, vol. 7, pp. 147470–147480, 2019.
- [12] M.-Z. Liu, Y.-Z. Xie, N. Dong, Z.-Y. Wang, and Y.-F. Yang, "Numerical analysis of nonuniform geoelectric field impacts on geomagnetic induction in pipeline networks," *IEEE Trans. Electromagn. Compat.*, vol. 64, no. 4, pp. 999–1009, 2022.
- [13] M.-z. Liu, Y.-z. Xie, Y.-h. Chen, R. Trincherro, and I. S. Stievano, "Modeling of induction in integrated power-gas systems due to geomagnetic disturbances," *IEEE Trans. Power Del.*, vol. 38, no. 6, pp. 3847–3859, 2023.
- [14] D. Chrysostomou, A. Dimitriou, N. D. Kokkinos, and C. A. Charalambous, "Short-term electromagnetic interference on a buried gas pipeline caused by critical fault events of a wind park: A realistic case study," *IEEE Trans. Ind Appl.*, vol. 56, no. 2, pp. 1162–1170, 2020.
- [15] C. M. Moraes, G. H. d. S. Matos, A. G. Martins-Britto, K. M. Silva, and F. V. Lopes, "Total AC interferences between a power line subject to a single-phase fault and a nearby pipeline with multilayered soil," *IEEE Trans. Electromagn. Compat.*, vol. 65, no. 2, pp. 585–594, 2023.
- [16] P. Lagace, J.-L. Houle, H. Greiss, and D. Mukhedkar, "Computer aided evaluation of pipeline current near toroidal HVDC ground electrodes," *IEEE Trans. Power Del.*, vol. 4, no. 1, pp. 216–222, 1989.
- [17] X. Meng, B. Zhang, Y. Liao, R. Li, B. Gong, and F. Cao, "Potential influence of ground return current from HVDC grounding electrode on buried pipeline," *Proc. Chin. Soc. Elect. Eng.*, vol. 39, no. 20, pp. 6113–6121, 2019.
- [18] Z. Yu, L. Liu, Z. Wang, M. Li, and X. Wang, "Evaluation of the interference effects of HVDC grounding current on a buried pipeline," *IEEE Trans. Appl. Supercond.*, vol. 29, no. 2, pp. 1–5, 2019.
- [19] B. Zhang, F. Cao, and X. Meng, "Evaluation of impressed potential on buried pipeline near HVDC grounding electrode considering polarization effect," *Chin. Soc. Elect. Eng. J. Power Energy Syst.*, early access, Jun. 25, 2021, doi:10.17775/CSEEJPES.2020.05870.
- [20] X. Li, J. Lu, F. Bai, F. Cao, and C. Li, "Modeling and calculation of the coupled voltage and current on the oil and gas pipeline from the HDVC/UHDC electrode grounding currents while considering the nonlinear polarization effect," *Proc. Chin. Soc. Elect. Eng.*, vol. 42, no. 3, pp. 1198–1209, 2022.
- [21] X. Li, J. Lu, F. Cao, F. Bai, and C. Li, "Corrosion effects of HVDC grounding currents on oil and gas pipelines under different soil resistivity conditions considering nonlinear polarization," *Power Syst. Technol.*, vol. 46, no. 12, pp. 5021–5028, 2022.
- [22] A. Zaboli, B. Vahidi, S. Yousefi, and M. M. Hosseini-Biyouki, "Evaluation and control of stray current in DC-electrified railway systems," *IEEE Trans. Veh. Technol.*, vol. 66, no. 2, pp. 974–980, 2017.
- [23] H.-J. Haubrich, B. Flechner, and W. Machczynski, "A universal model for the computation of the electromagnetic interference on earth return circuits," *IEEE Trans. Power Del.*, vol. 9, no. 3, pp. 1593–1599, 1994.
- [24] E. J. Dickinson and A. J. Wain, "The Butler-Volmer equation in electrochemical theory: Origins, value, and practical application," *J. Electroanal. Chem.*, vol. 872, 2020, Art. no. 114145.
- [25] C. Nucci, F. Rachidi, and M. Rubinstein, "Derivation of telegrapher's equations and field-to-transmission line interaction," in *Electromagnetic Field Interaction with Transmission Lines: From Classical Theory to HF Radiation Effects*. Southampton, UK: WIT Press, 2008, ch. 1, pp. 1–22.
- [26] C.-M. Liu, L.-G. Liu, and R. Pirjola, "Geomagnetically induced currents in the high-voltage power grid in China," *IEEE Trans. Power Del.*, vol. 24, no. 4, pp. 2368–2374, 2009.
- [27] Z. Du, Y.-z. Xie, and F. G. Canavero, "A Spice-compatible macromodel for field coupling to multiconductor transmission lines based on the analog behavioral modeling," *IEEE Trans. Electromagn. Compat.*, vol. 61, no. 6, pp. 1884–1890, 2019.
- [28] H. Xue, A. Ametani, J. Mahseredjian, and I. Kocar, "Generalized formulation of earth-return impedance/admittance and surge analysis on underground cables," *IEEE Trans. Power Del.*, vol. 33, no. 6, pp. 2654–2663, 2018.
- [29] A. De Conti, N. Duarte, R. Alipio, and O. E. Leal, "Small-argument analytical expressions for the calculation of the ground-return impedance and admittance of underground cables," *Electr. Power Syst. Res.*, vol. 220, 2023, Art. no. 109299.

- [30] A. De Conti, N. Duarte, and R. Alipio, "Closed-form expressions for the calculation of the ground-return impedance and admittance of underground cables," *IEEE Trans. Power Del.*, vol. 38, no. 4, pp. 2891–2900, 2023.
- [31] X.-F. Wang, Y. Song, and M. Irving, "Load flow analysis," in *Modern Power Systems Analysis*. Boston, MA: Springer US, 2008, pp. 71–128.
- [32] R. Arritt and B. Leonardi, "Geomagnetic disturbance (GMD) non-uniform field benchmark test case: Benchmarking geomagnetically induced currents with non-uniform geoelectric fields," *Electr. Power Res. Inst.*, Palo Alto, CA, Tech. Rep. 3002018766, 2020.



Min-zhou Liu (Member, IEEE) was born in Hebei, China, in 1995. He received the B.S. degree in electrical engineering from Xi'an Jiaotong University, Xi'an, China, in 2017. He is currently pursuing the Ph.D. degree in electrical engineering under the double degree program jointly supported by Xi'an Jiaotong University and Politecnico di Torino, Turin, Italy. His research interests include power system risk assessment, complex network, and electromagnetic effects.



Yan-zhao Xie (Senior Member, IEEE) received the Ph.D. degree in electrical engineering from Tsinghua University, Beijing, China, in 2005. He is currently a Professor of the School of Electrical Engineering, Xi'an Jiaotong University, Xi'an, China. Since 2016, he has been the Director of the National Center for International Research on Transient Electromagnetics and Applications. His research interests include electromagnetic compatibility, electromagnetic transients in power system, and high-power electromagnetics.



Yu-ying Wu was born in Qinghai, China, in 1996. She received the B.S. degree in electrical engineering from Beijing Jiaotong University, Beijing, China, in 2018. She is currently working toward the Ph.D. degree in electrical engineering with Xi'an Jiaotong University, Xi'an, China. Her research interests include electromagnetic transients and their protection.



Riccardo Trincherio (Member, IEEE) received the M.Sc. and Ph.D. degrees in electronics and communication engineering from the Politecnico di Torino, Turin, Italy, in 2011 and 2015, respectively. He is currently an Associate Professor with the EMC Group, Department of Electronics and Telecommunications, Politecnico di Torino. His research interests include the analysis of switching dc-dc converters, machine learning, and statistical simulation of circuits and systems.



Igor Simone Stievano (Senior Member, IEEE) received the master's degree in electronic engineering and the Ph.D. degree in electronics and communication engineering from the Politecnico di Torino, Turin, Italy, in 1996 and 2001, respectively. He is currently a Professor of electrical engineering with the Department of Electronics and Telecommunications, Politecnico di Torino. From 2017 to 2021, he was the Vice Rector of Academic and Scientific Activities of the joint campus of the Politecnico di Torino in Uzbekistan, Turin Polytechnic University in Tashkent. He has authored or coauthored more than 130 papers published in international journals and conference proceedings. His research interests include electromagnetic compatibility and signal integrity, with emphasis on modeling and simulation of digital circuits, transmission lines, PLC channels, switching converters, development of stochastic methods for the statistical simulation of circuits and systems, and the compact modeling of electrical and gas networks via a complex network paradigm and simplified graph-based approaches. He was the Program Co-Chair of the 20th and 21st IEEE Workshops on Signal and Power Integrity (SPI2016 and SPI2017).